SUPPLEMENTARY FIGURE LEGENDS

Figure S1, related to Figure 1. A) Coronal sections along the rostral (left) to caudal (right) axis through the forebrain of P30 WT (top) and cKO (bottom) mice, submitted to immunofluorescence staining for tdTomato (magenta) and counterstained with DAPI (blue). Scale bars, 250 μm. **B)** Quantification of the density of cells positive for tdTomato per mm^2 in the different subnuclei within the lateral septum of WT (green circles, n = 9) and cKO (purple squares, n = 9) mice. LSd, dorsal lateral septum; LSi, intermediate lateral septum; LSv, ventral lateral septum. **C)** Quantification of the density of cells positive for Zic per mm^2 in the lateral septum of WT (green circles, n = 4) and cKO (purple squares, n = 4) mice. **D)** Quantification of the area of the septum relative to the total area of its corresponding coronal brain section in WT (green circles, n = 6) and cKO (purple squares, n = 5) female mice. Measurements are normalized to the corresponding WT average. **E)** Quantification of the density of cells positive for tdTomato per mm^2 in the lateral septum of WT (green symbols, n = 5 males, 4 females) and cKO (purple symbols, n = 5 males, 4 females) mice, as in **Figure 1D**, separated by sex as indicated. **F)** Example images of the septa of P30 WT (left) and cKO (right) mice, submitted to immunofluorescence staining for Sox9 (green) and counterstained with DAPI (blue). Scale bars, 250 μm. **G)** Quantification of the density of cells positive for Sox9 per mm^2 in the lateral (left) and medial (right) septum of WT (green circles, n = 4) and cKO (purple squares, n = 4) mice. Unpaired t-tests with Welch's correction were performed; the p-values are shown above the corresponding compared sets of data: bold typeface indicates statistically significant ($p<0.05$) differences.

Figure S2, related to Figure 2. A) Quantification of the proportion (in %) of urocortin-3 perineuronal baskets surrounding tdTomato+ cells in the different subnuclei within the LS of WT (green circles, n = 8) and cKO (purple squares, n = 7) mice at P30. **B)** Quantification of fluorescence intensity in the different LS subnuclei of P30 WT (green circles, n = 8) and cKO (purple squares, n = 7) brains where urocortin-3 was detected by immunofluorescence staining, at the Section I and Section III levels along the rostrocaudal axis. **C)** Overview coronal images of the septum of P30 WT (left) and cKO (right) mice submitted to immunofluorescence staining for enkephalin (gray). Scale bars, 250 μm. **D)** Closeup view of the white dashed line boxes in **C**, showing the combined signals for enkephalin (green) and urocortin-3 (magenta), in the LS of WT (top) and cKO (bottom) mice. Scale bars, 50 μm. **E)** Quantification of fluorescence intensity in the different LS subnuclei of P30 WT (green circles, n = 8) and cKO (purple squares, n = 7) brains where enkephalin was detected by immunofluorescence staining, at three levels along the rostrocaudal axis (Sections I through III). **F)** Quantification of the density of enkephalin+ baskets per mm^2 in the different LS subnuclei, at three levels along the rostrocaudal axis (Sections I through III), in WT (green circles; n = 8, n = 5 and n = 5 for Sections I, II and III, respectively) and cKO (purple squares; n = 5, n = 4 and n = 3 for Sections I, II and III, respectively) mice. Unpaired t-tests with Welch's correction were performed; the p-values are shown above the corresponding compared sets of data: bold typeface indicates statistically significant ($p<0.05$) differences.

Figure S3, related to Figure 3. A) Example of injection site in the lateral septum of an Nkx2.1-Cre mouse subjected to retrograde monosynaptic circuit tracing, stained for GFP (green; expressed by *Nkx2.1*-lineage cells infected by the helper AAV) and counterstained with DAPI (blue). Scale bar, 500 μm. **B,C)** Examples of retrogradely labeled neurons in the ventral hippocampus of WT (**B**) and cKO (**C**) brains (corresponding to the same animals displayed in **Figure 3H** and **I**, respectively) injected with CTB-647 into the lateral septum. Scale bars, 250 μm.

Figure S4, related to Figure 4. A) Examples of coronal sections of the septum of WT (left) and cKO (right) age-matched control mice (i.e., not subjected to the forced restraint experiment), immunostained for c-Fos (green) and counterstained with DAPI (blue). **B)** Quantification of the density of c-Fos+ neurons per mm^2 in the entire LS of WT (green circles, n = 4) and cKO (purple squares, n = 4) control animals. **C)** Proportion of tdTomato+ neurons within the c-Fos+ population in the different subnuclei within the LS of WT (green circles, n = 4) and cKO (purple squares, n = 4) mice subjected to forced restraint. **D)** Proportion of tdTomato+ neurons within the c-Fos+ population in the LS of cKO mice, comparing untreated controls ('baseline', empty squares) and animals subjected to forced restraint ('restraint', full squares). **E)** Comparison of the density of c-Fos+ neurons in the LSi (top) and the LSv (bottom) of WT (green circles) and cKO (purple squares) animals subjected to forced restraint. Unpaired t-tests with Welch's correction were performed; the p-values are shown above the corresponding compared sets of data: bold typeface indicates statistically significant ($p<0.05$) differences.

Figure S5, related to Figure 5. A) Overview of the timeline used when performing anxiety-related behavior tests. **B-G)** Left, cartoons illustrating the outline of each behavior test; right, summary of the main anxiety-related readout for males and females. The behavioral tests performed were: **B**, light-dark box; **C**, open field; **D**, novel object; **E**, elevated plus-maze; **F**, social interaction; **G**, Y-maze. Unpaired t-tests with Welch's correction were performed; the p-values are shown above the corresponding compared sets of data: bold typeface indicates statistically significant ($p<0.05$) differences. **H, J)** Syllable usage in female (**H**) and male (**J**) WT mice during both parts of the experiment, with syllables most enriched in the TMT portion to the left, and in the Blank portion to the right. **I, K)** Syllable usage in female (**I**) and male (**K**) cKO mice during both parts of the experiment, with syllables most enriched in the TMT phase to the left, and in the Blank phase to the right. **L)** Syllable usage in male mice during the Blank portion of the experiment, with syllables most enriched in cKO mice to the left, and in WT to the right. **M)** Syllable usage in male mice during the TMT portion of the experiment, with syllables most enriched in cKO mice to the left, and in WT to the right. Data points in **H-M** represent the average ± 95% confidence interval of the proportion (in %) of test time spent using the corresponding syllable. Significantly different syllable usage (indicated by asterisks) was determined using a Kruskal-Wallis test, post-hoc

Dunn's two-sided test with permutation, and multiple comparisons correction using the Benjamini-Hochberg procedure with a false discovery rate of 0.05.

Figure S1

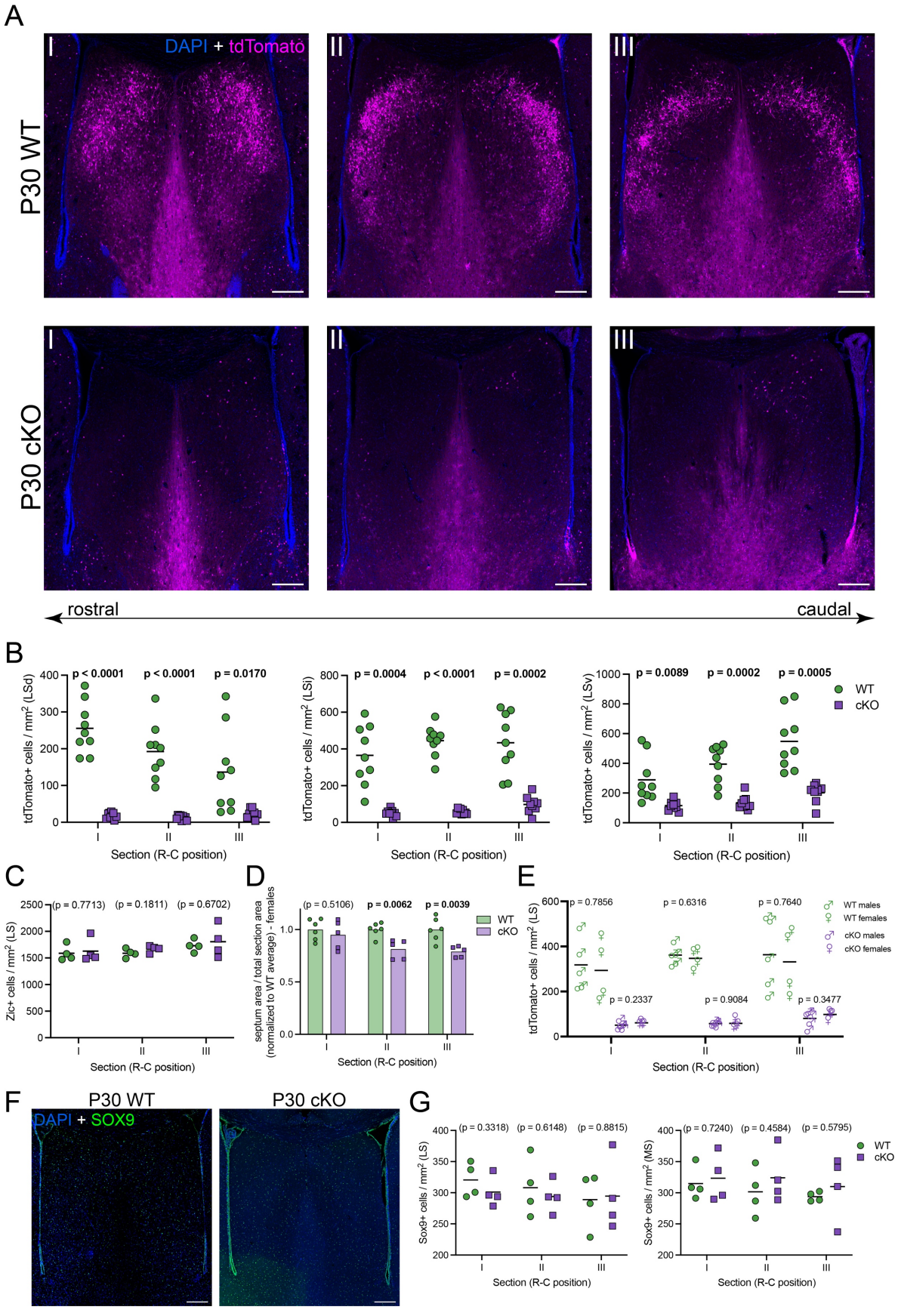

Figure S2

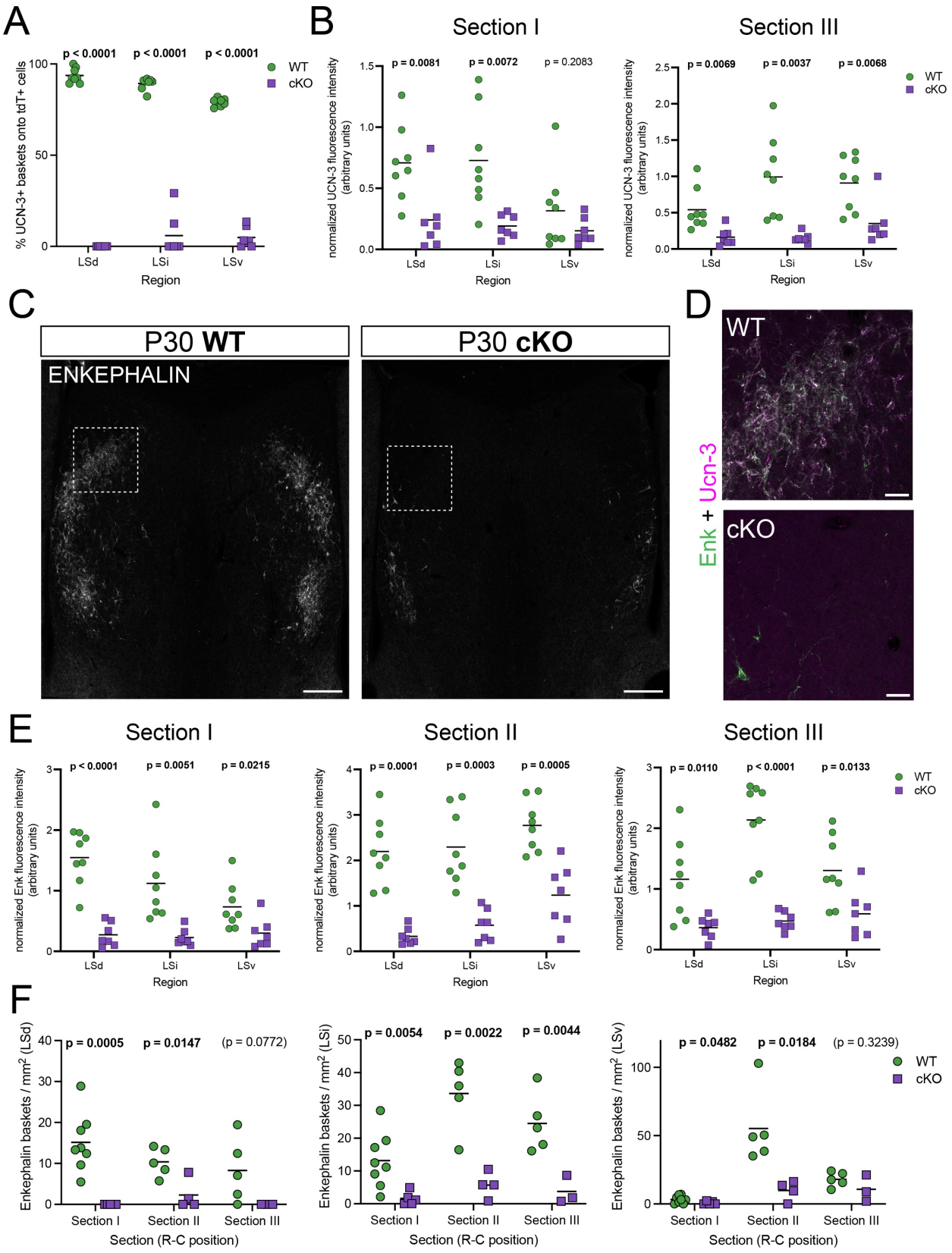

Figure S3

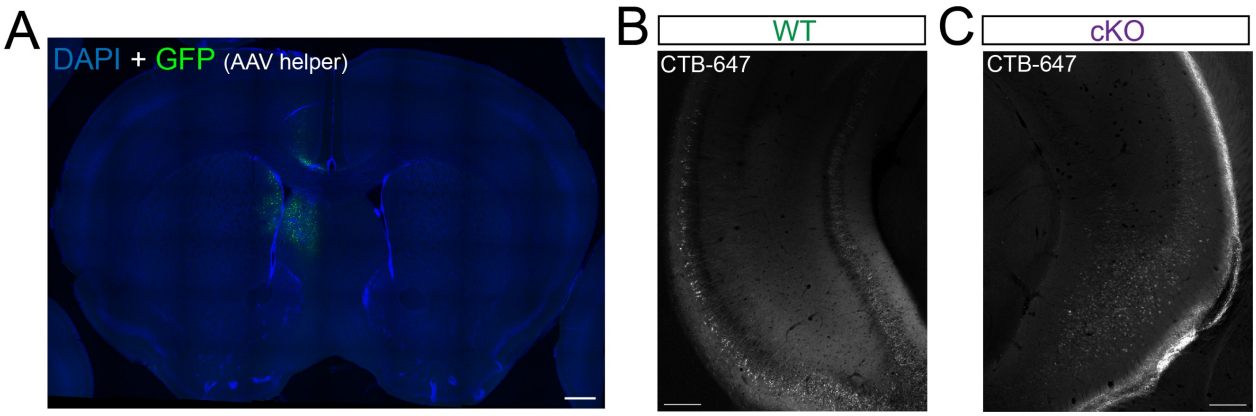

Figure S4

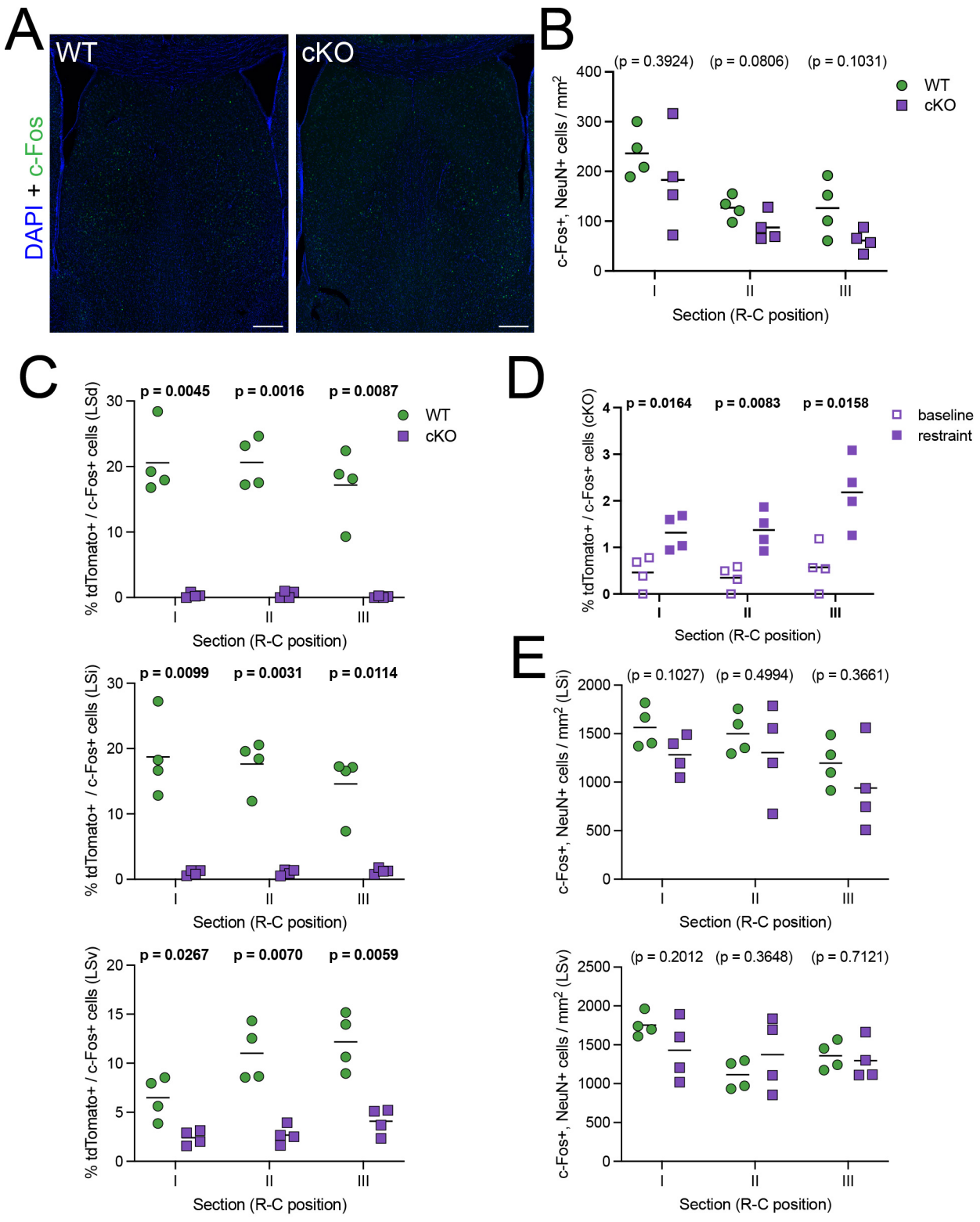

Figure S5